Primary Frequency Control Provision by Distributed Energy Resources in Active Distribution Networks

Ognjen Stanojev*, Justin Rüssli-Kueh *, Uros Markovic*, Petros Aristidou†, Gabriela Hug*
* EEH - Power Systems Laboratory, ETH Zurich, Switzerland
† Department of Electrical Engineering, Computer Engineering and Informatics, Cyprus University of Technology, Cyprus
Emails: {stanojev, markovic, hug}@eeh.ee.ethz.ch, justinr@student.ethz.ch, petros.aristidou@cut.ac.cy

***Abstract*—The rising share of renewable energy sources in electricity grids has strongly impacted the operation of both transmission and distribution systems. With the decommissioning of synchronous generators, the transmission systems are becoming less resilient to disturbances, while the proliferation of Distributed Energy Resources (DERs) in distribution networks has opened new possibilities for distribution system operators, enabling them to support the transmission system by offering ancillary services. This paper proposes a centralized controller for provision of Primary Frequency Control (PFC) by aggregations of DERs in active distribution networks. The controller aims to find optimal setpoint adjustments for DERs to regulate the power flow at the transmission system interconnection according to PFC provision requirements. At the heart of the proposed method lies a multi-period optimal power flow formulation, which accommodates different timescale dynamics of the employed DERs, as well as the network constraints. The active power required for provision of PFC is calculated using a recently developed frequency prediction model. Simulation results obtained from a dynamic model of the IEEE 33-bus system demonstrate the effectiveness of the proposed scheme.**

***Index Terms*—active distribution networks, distributed energy resources, primary frequency control, low-inertia systems**

I. Introduction

In the light of energy system decarbonization, the increased deployment of Renewable Energy Sources (RES) in power systems has given rise to new challenges and developments in both transmission and distribution systems. The safe operation of a transmission system is jeopardized by the decrease in rotational inertia and damping, leading to faster frequency dynamics and larger frequency deviations [1]. Consequently, control schemes for utility-scale batteries and inverter-interfaced RES, for instance Virtual Synchronous Machine [2] and droop-based control [3], have emerged to improve system resilience. Nevertheless, only a smaller share of the total RES capacity is connected to the transmission system and the majority of flexible units in the form of Distributed Energy Resources (DERs), such as Photovoltaic (PV), Battery Energy Storage Systems (BESS), and flexible loads are installed at low- and medium-voltage levels of Distribution Networks (DNs) [4]. Although DERs are presently used only to support the local operation of DNs, focusing on problems such as voltage rise and thermal overloading, a coordinated aggregation of a large number of flexible units in DNs offers great potential for ancillary service provision [5].

To effectively harness the collective flexibility from a large number of DERs, aggregation strategies including virtual power plants [6], DER clusters [7], and load aggregators [8] have recently been studied. Such paradigms utilize the existing communication infrastructure for network management, which is typically available in modern moderate scale DNs [9]. In this way, sufficient capacity of flexible units is aggregated for enabling active participation of DNs in energy and ancillary service markets and at the same time the security of supply in the local network is ensured.

The provision of ancillary services by active DNs has recently been the subject of numerous publications. Thus far, services such as voltage support [10], congestion management [11], and frequency control [7], [12]–[15] have been studied. While earlier works on provision of frequency control by active DNs consider only single unit types, e.g. BESS [12] or thermostatically controlled loads [13], more recent literature focuses on DER aggregations [7], [14]. In [7], a distributed algorithm for tracking the frequency control signal by a cluster of DERs is proposed. Although potential voltage violations are prevented by coordinating the reactive power of DERs in a local manner, line flow constraints are not included in the control design. A centralized control algorithm considering network constraints was proposed in [14]. The proposed methodology is based on a multi-period, chance-constrained Optimal Power Flow (OPF) formulation, where various frequency control products are offered by the active DN. Nevertheless, all of the aforementioned studies use steady-state modeling approaches for control design and verification, thus neglecting dynamic properties of system frequency and DERs. The significance of including DN dynamics was emphasized in [15], where a rule-based controller for provision of ancillary services was developed. Finally, while consideration of flexibility regions of individual DERs is commonly used in literature for quantification of DN flexibility [6], state-of-the-art research on ancillary service provision by DNs commonly neglects them.

This work proposes a centralized method for Primary Frequency Control (PFC) provision by active DNs through coordinated control of an aggregation of DERs. The controller aims to find the optimal active and reactive power setpoint adjustments for DERs, such as Diesel Generator (DG), PV and BESS units, to regulate the power flow at the transmission system interconnection according to PFC provision requirements. The cornerstone of the proposed method is a multi-period OPF formulation which ensures that the network constraints are respected during PFC provision, while incorporating different timescale dynamics of the employed DERs and their flexibility regions. The needed power for PFC provision is calculated for future time steps based on a recently developed frequency prediction model from [16], whereas the controller operates in Model Predictive Control (MPC) fashion to minimize the control effort and guarantee accurate reference tracking. Finally, contrary to the studies in [7], [14], the proposed control design is verified through time-domain simulations of the IEEE 33-bus system with detailed dynamic models of loads, network lines, and DER units.

The remainder of the paper is structured as follows. In Section II, the general structure of the proposed controller is introduced. Section III describes the multi-period receding

This research is supported by the Swiss National Science Foundation under NCCR Automation, grant agreement 51NF40_180545.

978-1-6654-3597-0/21/$31.00

horizon scheme used to find the optimal setpoint adjustments for DERs. Section IV showcases two case studies performed to verify the controller performance, whereas Section V concludes the paper.

II. PFC Provision by Active DNs

Traditionally, primary frequency control services are activated by a decentralized proportional controller within the speed governors of synchronous generators. Nevertheless, with the decreasing number of synchronous generators in the system, new frequency control providers are necessary. Modern active DNs are populated with a vast number of DERs and thus contain a substantial amount of operational flexibility, which is currently still an untapped resource. Multitudes of DERs can therefore be aggregated and controlled as a virtual power plant, providing frequency support through regulation of the DN's active power exchange with the transmission system. However, the range of DN's feasible operating points and resources is limited by static and dynamic properties of the network components and operational circumstances, which need to be taken into account in the control design. In the rest of this section, we first briefly review PFC provision rules and subsequently give an overview of the proposed centralized control scheme.

A. Primary Frequency Control

Properties and rules for provision of control reserves vary significantly between countries and control areas. Therefore, we employ common guidelines for the Continental Europe system (ENTSO-E) set forth in [17]. Active DNs with controlled DER aggregations would fit in this framework as Type C power-generating modules, which provide principle ancillary services to ensure security of supply. The needed PFC power $P(t) \in \mathbb{R}_{\geqslant 0}$, which depends on the frequency deviation $\Delta f(t) \in \mathbb{R}$ from the nominal $50\,\mathrm{Hz}$ and the contracted primary power $P_c \in \mathbb{R}$, can be expressed via the following droop expression:

$$P(t) = \begin{cases} P_c, & \Delta f(t) \leqslant -0.2\,\mathrm{Hz}, \\ -P_c \cdot \frac{\Delta f(t)}{0.2\,\mathrm{Hz}}, & -0.2\,\mathrm{Hz} < \Delta f(t) < 0.2\,\mathrm{Hz}, \\ -P_c, & \Delta f(t) \geqslant 0.2\,\mathrm{Hz}. \end{cases} \quad (1)$$

In Continental Europe, primary frequency control has to be fully activated within $15\,\mathrm{s}$ and sustained for the maximum duration of $15\,\mathrm{min}$. Although ENTSO-E recommends a narrow deadband to be implemented, it is neglected in this work for simplicity.

B. Proposed Control Structure

In this work, we consider a radial balanced DN represented by a connected graph $\mathcal{G}(\mathcal{N}, \mathcal{E})$, with $\mathcal{N} := \{0, 1, \ldots, N\}$ denoting the set of network nodes and $\mathcal{E} \subseteq \mathcal{N} \times \mathcal{N}$ the set of N network branches. The distribution network is populated with a number of DERs and loads, where $\mathcal{B} \subseteq \mathcal{N}$ indicates the subset of nodes with BESS, $\mathcal{P} \subseteq \mathcal{N}$ the subset of nodes with PV, and $\mathcal{D} \subseteq \mathcal{N}$ is the subset of nodes with DGs. The set of nodes with DERs is thus represented by the following set union $\mathcal{R} := \mathcal{B} \cup \mathcal{P} \cup \mathcal{D}$ of cardinality $N_R := |\mathcal{R}|$.

The proposed control structure is illustrated in Fig. 1. During normal operation, the DERs are operated by their respective local controllers $\mathcal{L}$, ensuring grid synchronization and reference tracking. In case of frequency deviations, the local controller setpoints are adjusted by the central DN controller such that the active power required for PFC is delivered. The central controller uses the available measurements to compute the optimal setpoint adjustments and is composed of an estimator, a frequency prediction module and a multi-period OPF procedure.

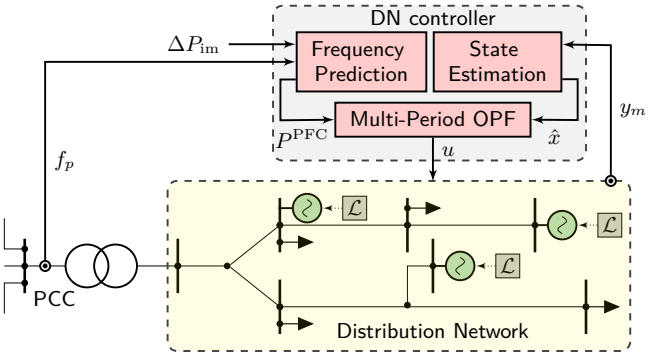

Fig. 1. Proposed control structure.

1) State Estimation: Measurements available across the DN such as bus voltages, branch currents and DER outputs are described by vector $y_m \in \mathbb{R}^m$, with $m \in \mathbb{N}$ being the number of measurements, and processed by the estimator to determine the state of the DN $\hat{x} \in \mathbb{R}^{2N}$. Since the focus of this work is not on DN estimation techniques, we assume that sufficient measurements are available across the DN such that its state can promptly be determined using network equations.

2) Frequency Prediction Module: A center of inertia frequency prediction model developed in [16] is adopted and complemented with the expression in (1) for prediction of the active power regulation to be delivered for PFC provision. Following the work in [18], a discrete time state space representation of the frequency prediction model can be derived as

$$Q_{k+1} = A_d Q_k + B_d \Delta P_{\mathrm{im}}, \qquad k = 1, 2, \ldots, H, \quad (2a)$$
$$f_k = C_d Q_k + f_p, \qquad k = 1, 2, \ldots, H, \quad (2b)$$

with $A_d \in \mathbb{R}^{2\times 2}$, $B_d \in \mathbb{Z}^2_{\geqslant 0}$ and $C_d \in \mathbb{R}^{1\times 2}_{\geqslant 0}$ describing the respective state space, $Q_k \in \mathbb{R}^2$ denoting the state vector at time step k, and $H \in \mathbb{N}$ being the number of considered time steps. Frequency measurement $f_p \in \mathbb{R}_{\geqslant 0}$ at the Point of Common Coupling (PCC) and active power imbalance magnitude $\Delta P_{\mathrm{im}} \in \mathbb{R}$ represent model inputs. The power imbalance magnitude can be determined either locally from frequency measurements, as discussed in [18], or using data-driven algorithms described in [19]. The state-space matrices are time-invariant and dependent on the inertia and governor constants of synchronous machines as well as the controller parameters of inverter-based generation participating in frequency control. Verification of the proposed frequency model can be found in [16], together with definitions and expressions of all relevant parameters. Prediction of the required active power regulation $P^{\mathrm{PFC}} \in \mathbb{R}^H$ for every time step can be subsequently computed by evaluating (1) based on the predicted frequency evolution.

Finally, outputs of the frequency prediction module and the estimator are passed to the multi-period OPF procedure which computes optimal setpoint adjustments for a future time horizon. Nevertheless, as the algorithm is implemented in MPC fashion, only setpoints $u \in \mathbb{R}^{2N_R}$ for the next step are applied to the local DER controllers and the rest is discarded. In the next controller time step, the process is repeated and the control loop continues until the measured frequency deviation is restored to zero by the units participating in automatic generation control.

III. Centralized Multi-Period OPF

In this section, the centralized multi-period OPF scheme used to compute the optimal DER setpoint adjustments is presented. Since computational efficiency is vital for applications involving real-time operation of distribution networks, several approximations are used in order to guarantee linearity of the constraint set. In addition, the objective function is selected to be quadratic, rendering the resulting optimization problem a quadratic program, which can be solved efficiently.

A. Objective Function

The objective function reflects the control goal of minimizing the total DER control effort and network losses over all time steps $\mathcal{H} := \{\hat{k}, \hat{k}+1, \dots, \hat{k}+H\}$ within the receding horizon of length $H \in \mathbb{N}$, with $\hat{k}$ being the current time step:

$$\begin{aligned}\min_{u} \quad & \sum_{k\in\mathcal{H}} \sum_{d\in\mathcal{R}} \left(C_{P_d} (\Delta P^{\star}_{d,k})^2 + C_{Q_d} (\Delta Q^{\star}_{d,k})^2 \right) + \\ & \sum_{k\in\mathcal{H}} \Delta P^{\text{loss}}_{k} + C_{\eta} \sum_{k\in\mathcal{H}} |\eta_k|,\end{aligned} \tag{3}$$

where $u \in \mathbb{R}^{2N_R \times H}$ is the vector of control variables, $\Delta P^{\star}_{d,k} \in \mathbb{R}$ and $\Delta Q^{\star}_{d,k} \in \mathbb{R}$ are the respective active and reactive power setpoint changes of the DER connected at node d at time step k, and $\Delta P^{\text{loss}}_{k} \in \mathbb{R}$ denotes the change in network losses at time step k. The coefficients $C_P \in \mathbb{R}_{\geqslant 0}$ and $C_Q \in \mathbb{R}_{\geqslant 0}$ are selected based on the following relationship:

$$C_{Q_r} \leqslant C_{P_p} \leqslant C_{P_d} \leqslant C_{P_b}, \quad r \in \mathcal{R}, p \in \mathcal{P}, d \in \mathcal{D}, b \in \mathcal{B}, \tag{4}$$

which establishes dispatch priorities of different DER types considering battery deterioration and fuel costs. Moreover, slack variable $\eta_k \in \mathbb{R}$ jointly with a large penalty constant $C_\eta \in \mathbb{R}_{\geqslant 0}$ is used to relax the PFC delivery constraint at each time step k, as will be discussed later in this section.

B. Power Flow Constraints

To take advantage of the radial DN structure, we employ the Backward/Forward Sweep (BFS) power flow model proposed in [20]. The method consists of the backward sweep where the branch currents $I^{\text{br}}_k \in \mathbb{C}^N$ are calculated using nodal current injections $I^{\text{inj}}_k \in \mathbb{C}^{N+1}$, and the forward sweep where the voltage drops over all branches $\Delta V_k \in \mathbb{C}^N$ are determined. Lastly, nodal voltages $V_k \in \mathbb{C}^N$ are updated and the process is repeated until convergence. Only a single BFS iteration is used to impose power flow constraints at every time step $k \in \mathcal{H}$ within the OPF framework, as follows:

$$I^{\text{br}}_k = BIBC \cdot I^{\text{inj}}_k, \tag{5}$$

$$\Delta V_k = BCBV \cdot I^{\text{br}}_k, \tag{6}$$

$$V_k = \mathbb{1}_N - \Delta V_k, \tag{7}$$

with $BIBC \in \{0,1\}^{(N+1)\times N}$ being a matrix populated with ones and zeros to capture the network topology, $BCBV \in \mathbb{C}^{N\times(N+1)}$ describing a complex matrix of the network branch impedances, and $\mathbb{1}_N$ denoting a column vector of ones of length N representing the per-unit voltage at the slack bus.

Nodal current injections $I^{\text{inj}}_{i,k}$ at each node $i \in \mathcal{N}$ and every time step $k \in \mathcal{H}$ are determined by

$$I^{\text{inj}}_{i,k} = \frac{P^{\text{inj}}_{i,k} + jQ^{\text{inj}}_{i,k}}{\bar{V}^{*}_{i,k}}, \tag{8}$$

where $j := \sqrt{-1}$ is the complex imaginary unit, $P^{\text{inj}}_{i,k} \in \mathbb{R}$ and $Q^{\text{inj}}_{i,k} \in \mathbb{R}$ are the respective net active and reactive power injections, and $\bar{V}^{*}_{i,k}$ is the complex conjugate of the voltage at node i. Note that the bar symbol indicates that the value is known *a priori*. Using only a single time step of the BFS algorithm has already been shown to be a valid approach for modeling power flows within an OPF framework, enabling circumvention of non-linearities which would otherwise be introduced by the AC power flow equations [14]. However, as discussed later, it is possible to include multiple iterations to improve the solution quality.

C. Power Balance Constraints

Active and reactive power balance constraints are imposed at every node by the following relationships:

$$P^{\text{inj}}_{i,k} = P^{\star}_{i,k} + \Delta P^{\star}_{i,k} - P^{\text{load}}_{i,k}, \qquad \forall i \in \mathcal{N}, \forall k \in \mathcal{H}, \tag{9}$$

$$Q^{\text{inj}}_{i,k} = Q^{\star}_{i,k} + \Delta Q^{\star}_{i,k} - Q^{\text{load}}_{i,k}, \qquad \forall i \in \mathcal{N}, \forall k \in \mathcal{H}, \tag{10}$$

where $P^{\text{load}}_{i,k} \in \mathbb{R}$ and $Q^{\text{load}}_{i,k} \in \mathbb{R}$ are active and reactive load power consumption, and $P^{\star}_{i,k} \in \mathbb{R}$ and $Q^{\star}_{i,k} \in \mathbb{R}$ are the initial DER active and reactive power setpoints.

D. Network Losses Approximation

The change in network losses resulting from adjustment of DER setpoints at every time step $k \in \mathcal{H}$ is approximated by a linear relationship of the following form:

$$\Delta P^{\text{loss}}_{k} \approx \sum_{(l,m)\in\mathcal{E}} \text{Re}(I^{*}_{k,l,m} \cdot \bar{I}_{k,l,m}) \cdot R_{l,m} - \bar{P}^{\text{loss}}_{k}, \tag{11}$$

with $I_{k,l,m} \in \mathbb{C}$ being the branch current connecting nodes l and m, $R_{l,m} \in \mathbb{R}_{\geqslant 0}$ representing the line resistance, $\bar{P}^{\text{loss}}_{k} \in \mathbb{R}_{\geqslant 0}$ and $\bar{I}_{k,l,m} \in \mathbb{C}$ denoting the network losses and branch current prior to applying setpoint changes to DERs. While only negligible errors are introduced by the approximation, computational advantages are achieved as a result of linearity of the loss approximation.

E. PFC Delivery Constraint

To ensure that the DN provides the needed amount of PFC, the current $I_{k,0,1} \in \mathbb{R}$ of the feeder branch (i.e., the line connecting nodes 0 and 1) at time step k is constrained by

$$I_{k,0,1} = \bar{I}_{0,1} - (P^{\text{PFC}}_{k} - \bar{P}_{\text{DN}}) + \eta_k, \quad \forall k \in \mathcal{H}, \tag{12}$$

where $\bar{I}_{0,1} \in \mathbb{R}$ is the most up-to-date feeder current measurement, P^{PFC}_{k} is the active power needed for PFC delivery predicted by (2) for future time steps, and $\eta_k \in \mathbb{R}_{\geqslant 0}$ is the slack variable used to relax the constraint and corresponds to undelivered PFC power. The PFC power already provided by the DN $\bar{P}_{\text{DN}} \in \mathbb{R}$ is calculated as the difference between the initial DN consumption and the present consumption adjusted as a result of the PFC delivery. Considering that the voltage at the feeder bus is assumed to be 1 p.u., direct relationship between current and power can be established.

F. Voltage and Thermal Loading Constraints

Considering the dominantly resistive nature of DN lines, one can assume that the angles of the bus voltages deviate only slightly from the reference angle. Therefore, it suffices to constrain the real part of bus voltages $V_{i,k} \in \mathbb{C}$, as follows:

$$V^{\min}_{i} \leqslant \text{Re}(V_{i,k}) \leqslant V^{\max}_{i}, \qquad \forall i \in \mathcal{N}, \forall k \in \mathcal{H}, \tag{13}$$

where $V_i^{\min} \in \mathbb{R}_{\geqslant 0}$ and $V_i^{\max} \in \mathbb{R}_{\geqslant 0}$ are the minimum and maximum allowed voltage magnitudes at every node. The thermal limit constraints are imposed by limiting the branch current magnitudes:

$$|I_{k,l,m}| \leqslant I_{l,m}^{\max}, \qquad \forall (l,m) \in \mathcal{E}, \forall k \in \mathcal{H}, \tag{14}$$

with $I_{l,m}^{\max}$ being the maximum admissible current for the branch connecting nodes l and m. To preserve linearity of the constrains, we employ a piecewise linear approximation of the quadratic current constraint, as suggested in [21].

G. DER Constraints

1) Flexibility Regions: The active and reactive power flexibility of DERs is constrained to their admissible regions, which are assumed to be constant for the duration of the PFC provision, as follows:

$$(P_{d,k}^{\star} + \Delta P_{d,k}^{\star}, Q_{d,k}^{\star} + \Delta Q_{d,k}^{\star}) \in \mathcal{F}_d, \quad \forall d \in \mathcal{R}, k \in \mathcal{H}, \tag{15}$$

where the flexibility region $\mathcal{F}_d = \{x \in \mathbb{R}^2 : A_d x \leqslant b_d\}$ is modeled as a polytope with $n \in \mathbb{N}$ edges defined by $A_d \in \mathbb{R}^{n \times 2}$ and $b_d \in \mathbb{R}^{n \times 1}$.

2) DG Dynamics: The dynamics pertaining to active power ramping of BESS and PV units are assumed to be faster than that of the control sampling and are therefore neglected. Nonetheless, the governor dynamics of DG units are considered by including the following expressions in the OPF formulation:

$$P_{d,k+1} = a(P_{d,k}^{\star} + \Delta P_{d,k}^{\star}) + (1-a) P_{d,k}, \forall d \in \mathcal{D}, k \in \mathcal{H}, \tag{16}$$

with $P_{d,k} \in \mathbb{R}$ representing the actual DG power output at time step k, and $a := 1 - e^{-T_s/T_g} \in \mathbb{R}_{\geqslant 0}$ being a constant defined by the controller sampling period $T_s \in \mathbb{R}_{\geqslant 0}$ and the governor time constant $T_g \in \mathbb{R}_{\geqslant 0}$.

3) BESS State of Charge: The state of charge $\chi_{b,k} \in \mathbb{R}$ of every BESS $b \in \mathcal{B}$ at each time step $k \in \mathcal{H}$ is modelled as

$$\chi_{b,k+1} = \chi_{b,k} - T_s \cdot \frac{P_{b,k}^{\star} + \Delta P_{b,k}^{\star}}{E_b}, \tag{17}$$

$$\chi_b^{\min} \leqslant \chi_{b,k} \leqslant \chi_b^{\max}, \tag{18}$$

with $E_b \in \mathbb{R}_{\geqslant 0}$ being the battery energy capacity. Furthermore, the limits on maximal charge $\chi_b^{\max} \in \mathbb{R}$ and discharge $\chi_b^{\min} \in \mathbb{R}$ of each BESS are enforced in (18).

H. Solution Algorithm

The complete solution algorithm, including an iterative BFS-OPF procedure and a model predictive control loop, is presented in Fig. 2. The algorithm is initiated upon a detection of frequency deviation and a subsequent measurement of the corresponding disturbance magnitude. In the next step, the estimation of network states is performed using the available DN measurements and the power required for PFC provision is predicted based on the measured power imbalance for a number of future time steps. The multi-period OPF presented in this section is then solved to obtain the optimal DER setpoints. However, since only a single BFS iteration is used to model the DN power flow, the solution can be refined through an iterative procedure as suggested in [14]. Namely, after the BFS-OPF solution, a full, non-linear, BFS power flow is solved to obtain the voltages. The multi-period BFS-OPF is then performed again using the updated voltage values from the full BFS. The iterative BFS-OPF procedure is repeated until the difference between BFS and OPF voltages at every time step

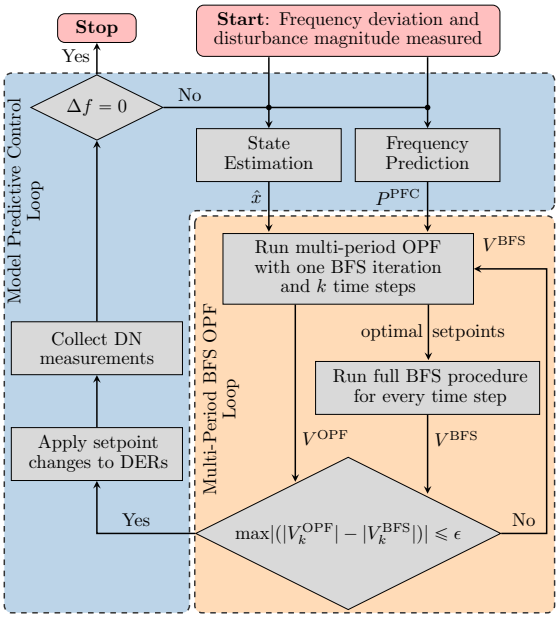

Fig. 2. Overview of the complete solution algorithm.

k becomes sufficiently small. The algorithm is implemented in an MPC fashion, as only setpoints for the first time step are applied to local DER controllers and the rest are discarded. The MPC loop continues until the frequency is restored to its nominal value.

IV. Results

The proposed control scheme has been implemented and evaluated on the IEEE 33-bus network [22], presented in Fig. 3. The system has been modified by adding PV units at nodes $\mathcal{P} = \{3, 18\}$, BESS at nodes $\mathcal{B} = \{8, 30\}$ and a DG at node $\mathcal{D} = \{25\}$. Polytopes of individual flexibility regions of the DERs are presented in Fig. 4, where crosses indicate their initial operating points. The per-unit system used throughout this work is defined by the base power of 1 MW and base voltage of 12.66 kV, and the storage capacity of BESS units is set to 260 kWh. The two PV systems and the two BESS are identically parametrized to examine the influence of their placement on the network behavior during the provision of PFC. The network is operated slightly below the nominal conditions, with the total load consumption amounting to 3.9 MW. The minimum and maximum acceptable voltages at each bus are set to 0.9 and 1.1 p.u., respectively, and the thermal loading limit of each line are set to 120% of the nominal value.

The simulations are performed in MATLAB Simulink using the Simscape Power System environment. The network lines

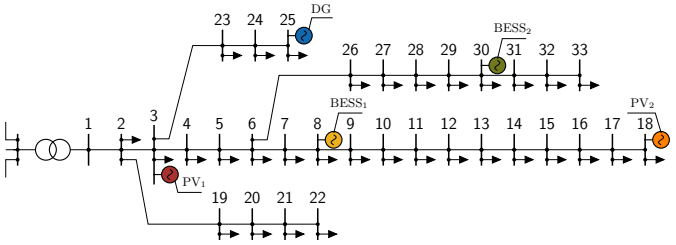

Fig. 3. Modified IEEE 33-bus system, with DERs placed at nodes 3, 8, 18, 25 and 30.

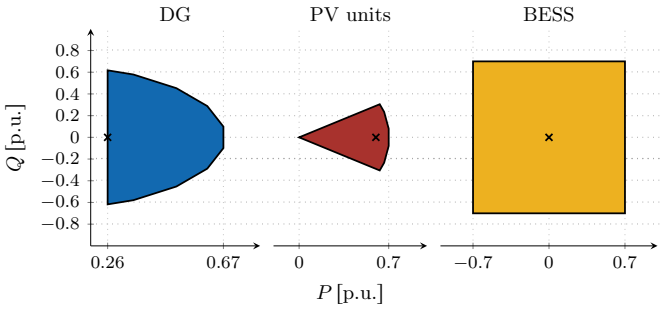

Fig. 4. Flexibility regions of the DG, PV and BESS units represented in the P-Q plane, with crosses indicating their initial operating points.

are modeled as three-phase, π-sections, the low voltage feeders as composite loads, and the transmission network as three-phase Thevinin equivalent with a controllable voltage source. For the diesel generator, we consider a 6^{th} order synchronous machine with diesel governor ($T_g = 1\,\text{s}$) and an excitation system including a reactive power control loop. Furthermore, PV and BESS units are represented by *grid-feeding* inverters, including a phase locked loop, a power measurement, a current control loop with a time constant of $100\,\text{ms}$, and an averaged switching unit.

The controller sampling period is set to $T_s = 250\,\text{ms}$ in order to account for the time needed to compute the optimal setpoints. Since the focus of this work is on the control problem, potential issues associated with the communication infrastructure are neglected. The multi-period OPF procedure is run for four future time steps (i.e. a horizon length of $1\,\text{s}$), thus making a trade-off between the controller performance and computational effort. Modelling of the optimization procedure was done in YALMIP [23] and CPLEX was used as the solver. The average solver time required for the solution of the iterative BFS-OPF procedure is around $100\,\text{ms}$, with the computations performed on an Intel i7-8850H processor.

In the following, the simulation results from two case studies are detailed. The case studies focus on either a positive or a negative step change in active power injection at a node in the transmission system, leading to a frequency deviation which necessitates the PFC activation. Furthermore, it is assumed that the active DN has sold $P_c = 1.5\,\text{p.u.}$ of primary control reserve in the ancillary service market, which has to be supplied according to the PFC dispatch rules in (1).

A. Negative Frequency Deviation

In this section, the controller performance for a loss of generation of $850\,\text{MW}$ in the transmission system is analyzed, which leads to frequency deviation shown in Fig. 5. Using the frequency prediction model in (2) and the frequency deviation measurement, the active power required to be supplied by the DN for PFC provision can be calculated, as indicated by the grey PFC line.

It can be observed that, under the proposed control scheme, the DN is capable of accurately supplying the needed active power according to the PFC provision requirements. The contribution of the PV units is minor since their upward flexibility is limited. As a result of the slow ramping of the DG and the low contribution from PVs, the residual power needs to be provided by BESS which are the most expensive units participating in PFC provision. The two BESS and the two PV units are dispatched identically, suggesting that their different placement in the network has no influence on PFC provision in this case study.

Furthermore, Fig. 5 depicts the plots of active and reactive power setpoints computed by the controller, where the applied setpoints are marked by triangles or rectangles and future anticipation of the setpoints by the controller is indicated by grey lines. Interestingly, the MPC anticipations do not coincide with the resulting solution over the complete horizon. In later time steps, the multi-period OPF aims to decrease the power setpoint of the DG and compensate the missing power by dispatching the BESS. The reason for such behavior is the short length of the prediction horizon and slow ramp-down of the DG power output. The utilization of the reactive power is only marginal and is attempting to impact the network voltages such that the network losses are minimized. Moreover, one can notice a rising trend in bus voltages resulting from the network deloading. Nevertheless, no voltage limits are reached.

B. Positive Frequency Deviation

Figure 6 illustrates the controller performance for a load loss of $850\,\text{MW}$, leading to a positive frequency deviation. Similarly to the previous case study, the active power requirement for provision of PFC can be calculated by means of the prediction model and the observed frequency deviation, and is indicated by the grey PFC_{ref} line in Fig. 6. As can be seen from the figure, the DN fails to provide the required support to the transmission system in the interval between $1\,\text{s}$ and $3\,\text{s}$.

Such behavior can be understood by observing the dispatch of individual DERs and the evolution of bus voltages and

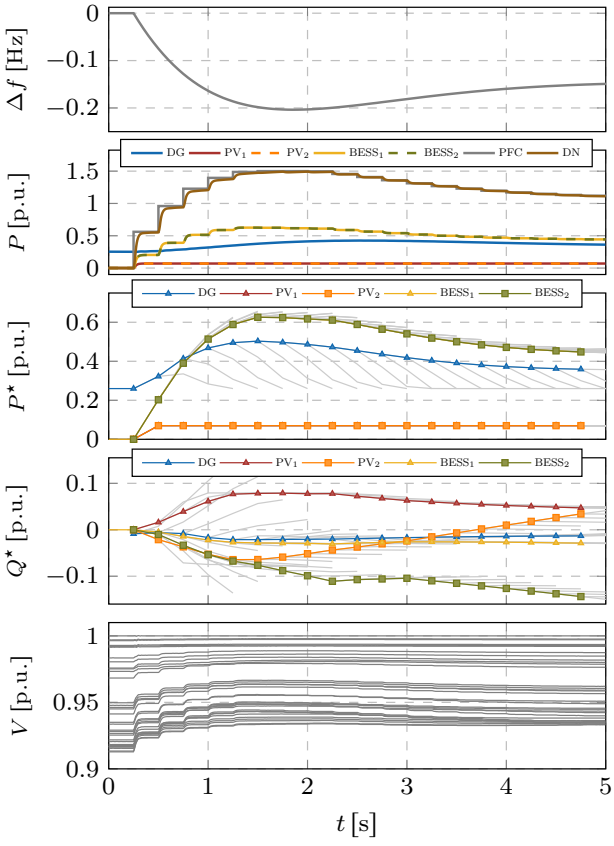

Fig. 5. Time-domain response after a generation loss: (i) frequency deviation; (ii) active power outputs; (iii) active power setpoints; (iv) reactive power setpoints; and (v) nodal voltages.

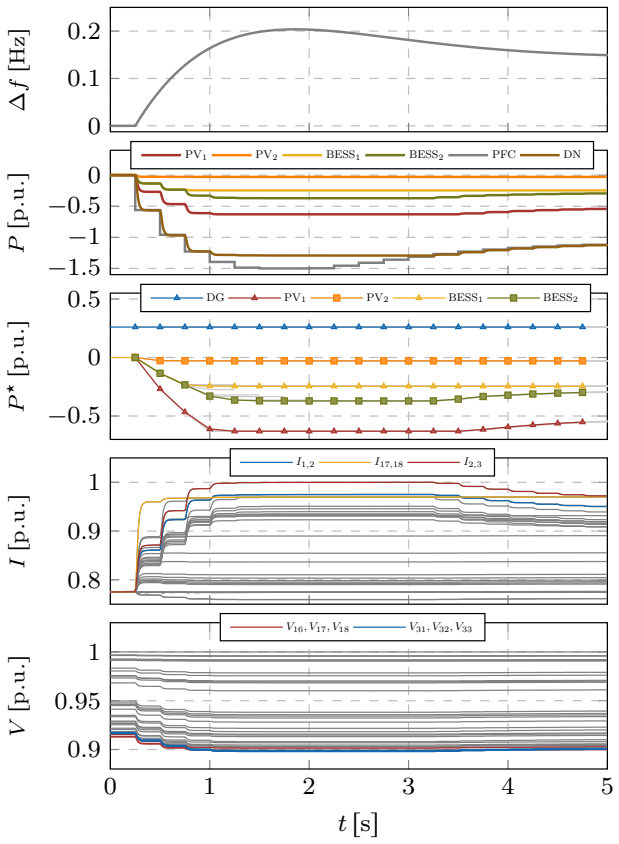

Fig. 6. Positive frequency deviation case study results showing plots of: (i) frequency deviation; (ii) active power outputs; (iii) active power setpoints; (iv) bus voltages; and (v) branch currents normalized by their thermal limits.

branch currents. Firstly, the DG remains at its minimal power output as it cannot be quickly turned off. The active power outputs of the PV and BESS units are now very different and depend on their placement in the DN. Namely, PV_2 is unable to curtail its production as the voltage limits at nodes 16, 17, and 18 are reached. Similarly, BESS_2 is unable to absorb more power as the voltage limits at nodes 31, 32, and 33 are binding. Although the power consumption of BESS_1 and PV_1 is not limited by voltage constraints, the saturation of their output occurs as a result of the thermal limit on the branch connecting nodes 2 and 3 being reached. Note that the reactive power output of DERs was negligible and hence has been omitted. This case study points out that the considered DN cannot provide enough negative PFC due to branch current and bus voltage limitations. In the worst-case scenario, approximately 0.3 p.u. of active power was not delivered. However, it also shows that the MPC algorithm is capable of accounting for bus voltage and line flow limits.

V. Conclusion

This paper introduces a novel centralized controller to aggregate and dispatch DERs in an active DN for provision of PFC. The controller collects measurements across the DN and employs a frequency prediction model to estimate the needed primary power after a disturbance. The active and reactive power setpoints are determined by solving a multi-period OPF, whose solutions are refined by an iterative OPF-BFS procedure. Different dynamics of DERs and network constraints are taken into account in the multi-period solution to gain a superior dispatch. In the two presented case studies, the controller successfully provided realistic and sensible power setpoints for the DERs in real-time. The limitations of the DN as a frequency control provider are exhibited by the fact that the DN can supply more positive primary power than negative. In addition, the preexisting bottlenecks in the grid are severely influenced by the placement of DERs in the DN.

References

[1] U. Markovic, O. Stanojev, P. Aristidou, E. Vrettos, D. S. Callaway, and G. Hug, "Understanding Small-Signal Stability of Low-Inertia Systems," *IEEE Transactions on Power Systems*, pp. 1–1, 2021.

[2] Q. C. Zhong and G. Weiss, "Synchronverters: Inverters that mimic synchronous generators," *IEEE Transactions on Industrial Electronics*, vol. 58, no. 4, pp. 1259–1267, April 2011.

[3] U. Markovic, O. Stanojev, P. Aristidou, and G. Hug, "Partial grid forming concept for 100% inverter-based transmission systems," in *IEEE PES General Meeting*, Aug 2018, pp. 1–5.

[4] B. Bayer, P. Matschoss, H. Thomas, and A. Marian, "The German experience with integrating photovoltaic systems into the low-voltage grids," *Renewable Energy*, vol. 119, pp. 129–141, 2018.

[5] N. Hatziargyriou *et al.*, "Contribution to Bulk System Control and Stability by Distributed Energy Resources connected at Distribution Network," IEEE PES, Tech. Rep., 2017.

[6] S. Riaz and P. Mancarella, "On feasibility and flexibility operating regions of virtual power plants and tso/dso interfaces," in *2019 IEEE Milan PowerTech*, 2019, pp. 1–6.

[7] Z. Tang, T. Liu, C. Zhang, Y. Zheng, and D. J. Hill, "Distributed control of active distribution networks for frequency support," in *2018 Power Systems Computation Conference (PSCC)*, 2018, pp. 1–7.

[8] Z. Tang, D. J. Hill, T. Liu, and H. Ma, "Hierarchical voltage control of weak subtransmission networks with high penetration of wind power," *IEEE Transactions on Power Systems*, vol. 33, no. 1, pp. 187–197, 2018.

[9] D. E. Olivares *et al.*, "Trends in microgrid control," *IEEE Transactions on Smart Grid*, vol. 5, no. 4, pp. 1905–1919, 2014.

[10] G. Valverde, D. Shchetinin, and G. Hug-Glanzmann, "Coordination of Distributed Reactive Power Sources for Voltage Support of Transmission Networks," *IEEE Transactions on Sustainable Energy*, vol. 10, no. 3, pp. 1544–1553, 2019.

[11] K. Knezović, M. Marinelli, P. Codani, and Y. Perez, "Distribution grid services and flexibility provision by electric vehicles: A review of options," in *2015 50th International Universities Power Engineering Conference (UPEC)*, 2015, pp. 1–6.

[12] M. Koller, T. Borsche, A. Ulbig, and G. Andersson, "Review of grid applications with the zurich 1mw battery energy storage system," *Electric Power Systems Research*, vol. 120, pp. 128 – 135, 2015.

[13] E. Vrettos and G. Andersson, "Combined load frequency control and active distribution network management with thermostatically controlled loads," in *2013 IEEE SmartGridComm*, 2013, pp. 247–252.

[14] S. Karagiannopoulos *et al.*, "Active Distribution Grids Offering Ancillary Services in Islanded and Grid-Connected Mode," *IEEE Transactions on Smart Grid*, vol. 11, no. 1, pp. 623–633, 2020.

[15] D. Mayorga Gonzalez *et al.*, "Dynamic Behaviour of Distribution Networks with TSO-DSO Interconnection Power Flow Control," in *IREP 2017 Symposium*, Portugal, 2017.

[16] U. Markovic, Z. Chu, P. Aristidou, and G. Hug, "LQR-based adaptive virtual synchronous machine for power systems with high inverter penetration," *IEEE Transactions on Sustainable Energy*, vol. 10, no. 3, pp. 1501–1512, 2019.

[17] ENTSO-E, "Frequency Sensitive Mode - Guidance document for national implementation for network codes on grid connection," 2018.

[18] O. Stanojev, U. Markovic, P. Aristidou, G. Hug, D. S. Callaway, and E. Vrettos, "MPC-Based Fast Frequency Control of Voltage Source Converters in Low-Inertia Power Systems," *IEEE Transactions on Power Systems*, pp. 1–1, 2020.

[19] O. Stanojev, U. Markovic, E. Vrettos, P. Aristidou, D. Callaway, and G. Hug, "Enhanced MPC for Fast Frequency Control in Inverter-Dominated Power Systems," in *2020 International Conference on Smart Energy Systems and Technologies (SEST)*, 2020, pp. 1–6.

[20] Jen-Hao Teng, "A direct approach for distribution system load flow solutions," *IEEE Transactions on Power Delivery*, vol. 18, no. 3, pp. 882–887, 2003.

[21] Z. Yang, H. Zhong, Q. Xia, A. Bose, and C. Kang, "Optimal power flow based on successive linear approximation of power flow equations," *IET Generation, Transmission Distribution*, vol. 10, no. 14, pp. 3654–3662, 2016.

[22] M. E. Baran and F. F. Wu, "Network reconfiguration in distribution systems for loss reduction and load balancing," *IEEE Transactions on Power Delivery*, vol. 4, no. 2, pp. 1401–1407, April 1989.

[23] J. Löfberg, "Yalmip : A toolbox for modeling and optimization in matlab," in *Proceedings of the CACSD Conference*, Taiwan, 2004.